Supplementary material (in CDS)

Figure 5: Kinematic distributions of the D^{*+} momentum p and transverse momentum p_T before (left) and after (right) the reweighting procedure for $D^0 \to K^- K^+$ (black line) and $D^0 \to \pi^- \pi^+$ (red dots) candidates. The distributions are normalised to unit area. The histograms show the distributions of signal candidates after background subtraction.
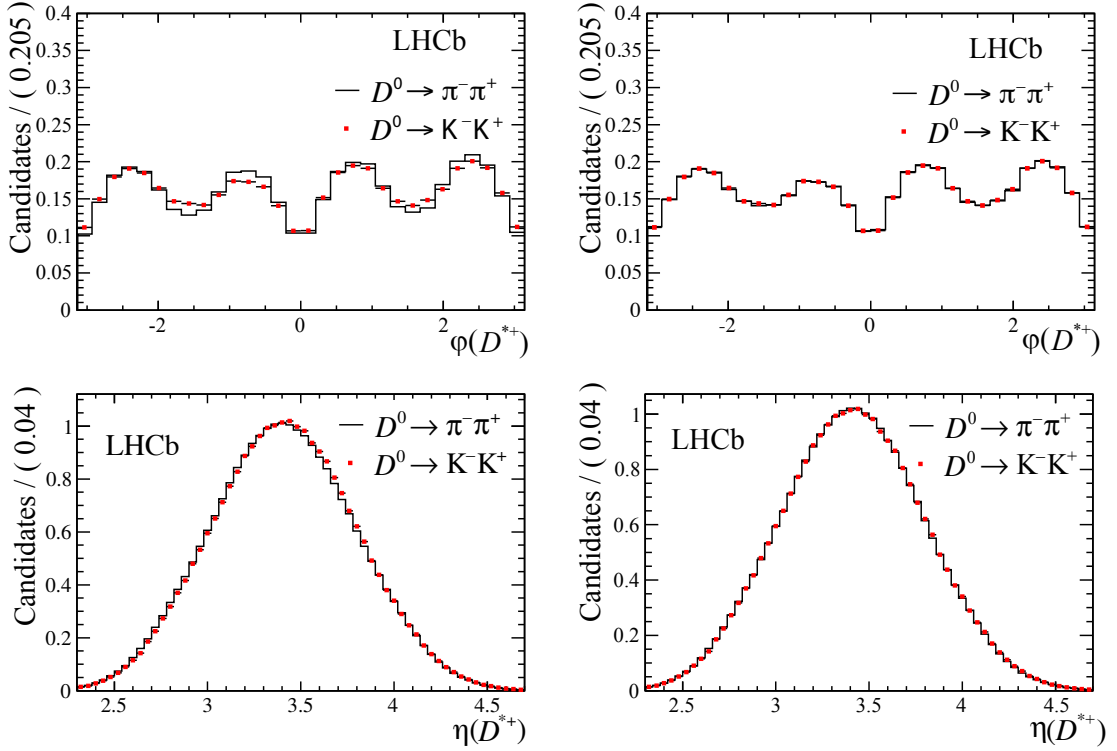
Figure 6: Kinematic distributions of the D^{*+} azimuthal angle φ and pseudorapidity η before (left) and after (right) the reweighting procedure for $D^0 \to K^- K^+$ (black line) and $D^0 \to \pi^- \pi^+$ (red dots) candidates. The distributions are normalised to unit area. The histograms show the distributions of signal candidates after background subtraction.
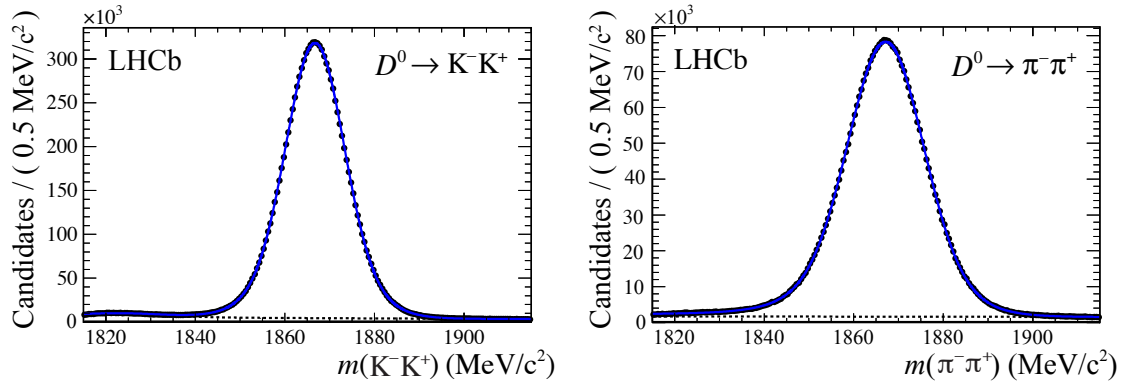

Figure 7: Fit to the (left) $m(K^- K^+)$ and (right) $m(\pi^- \pi^+)$ spectra for D^{*+} candidates passing the selection and satisfying $0.2 < \delta m < 12$ MeV/c^2. The dashed line corresponds to the background component in the fit. Only $D^0 \to K^- K^+$ and $D^0 \to \pi^- \pi^+$ candidates lying in the windows 1850–1884 MeV/c^2 and 1845–1889 MeV/c^2, respectively, are used for the final result.
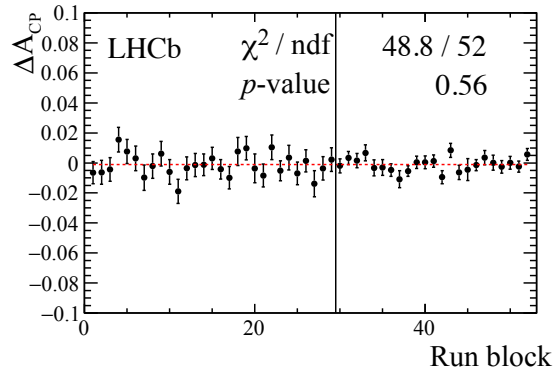
Figure 8: Time-dependence of ΔA_{CP}. The data are divided into 52 bins, and the value of ΔA_{CP} is measured in each bin. The uncertainties are statistical only. The horizontal red-dashed line shows the result for the combined sample. The χ^2/ndf, the corresponding p-value and the red-dashed line reported on the figures are the results of a fit to the ΔA_{CP} values with a horizontal line. The central value of the fit is consistent with the baseline result. The vertical dashed line separates the two years of data taking. No dependence on run block is observed.
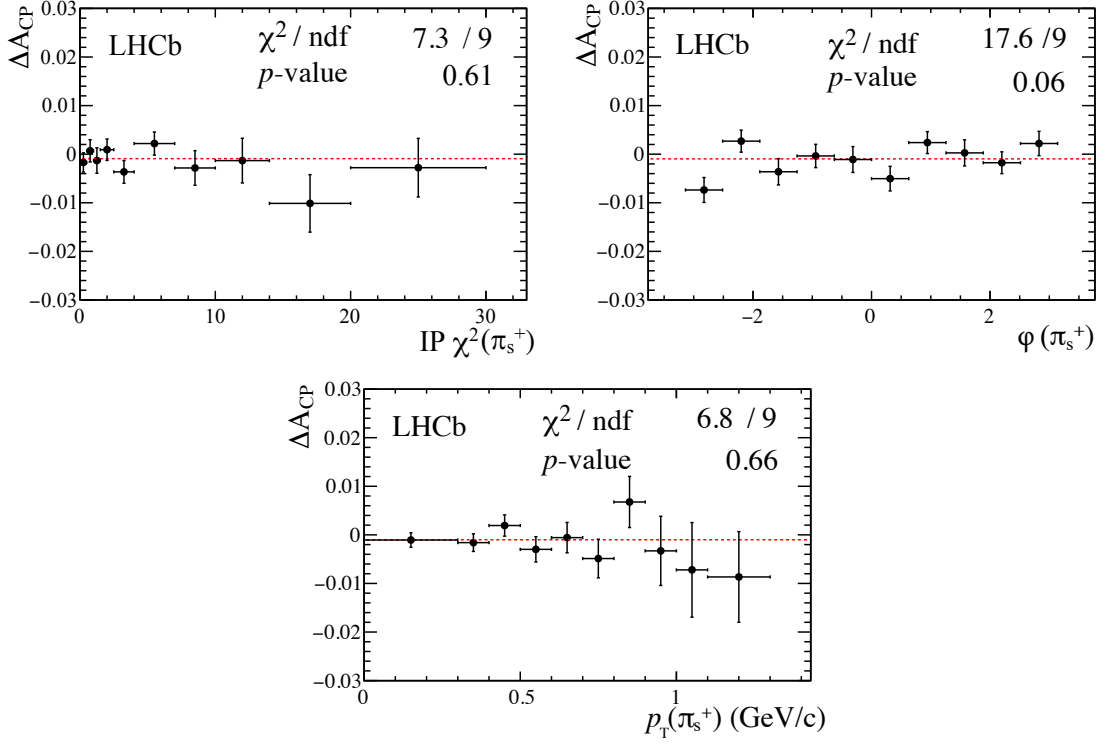
Figure 9: Dependence of ΔA_{CP} on soft pion IP χ^2 (top left), azimuthal angle, φ (top right), and transverse momentum, p_T (bottom). The data are divided into 10 bins, and the value of ΔA_{CP} is measured in each bin. The last bin includes all overflow events, except in the case of $\varphi(\pi_s^+)$. The uncertainties are statistical only. The χ^2/ndf, the corresponding p-value and the red-dashed line reported on the figures are the results of fits to the ΔA_{CP} values with a horizontal line. The central value of the fit is consistent with the baseline result. No dependencies on the variables are observed.
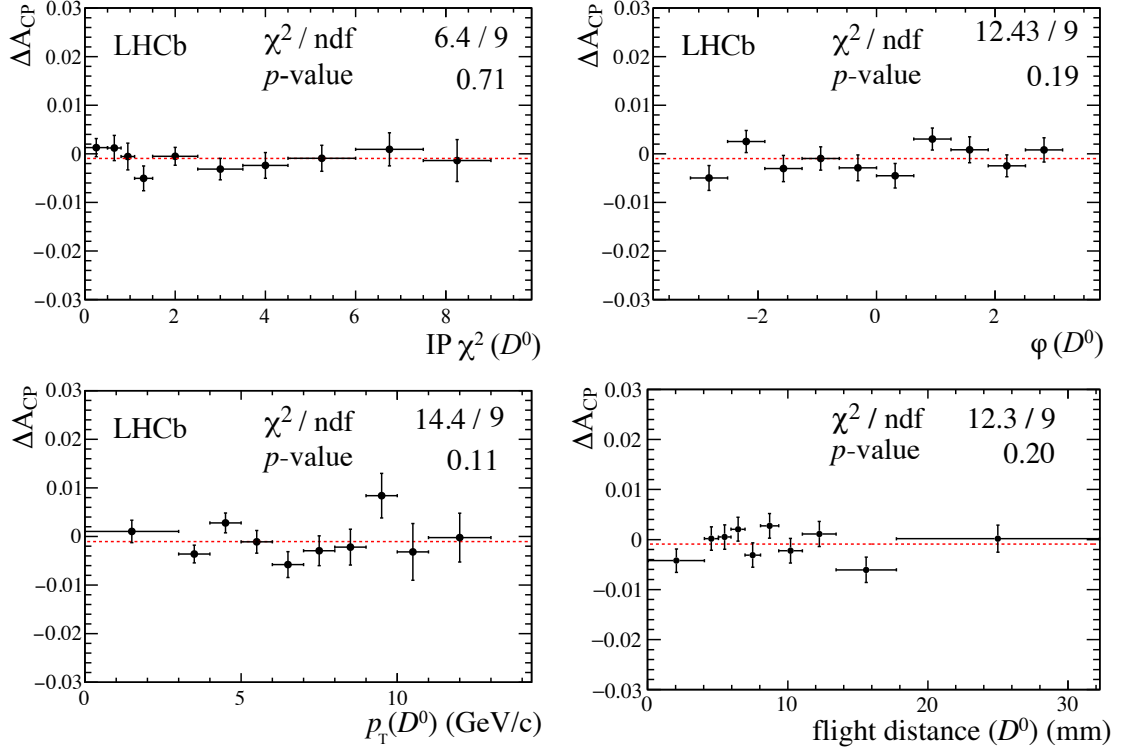
Figure 10: Dependence of ΔA_{CP} on the smallest D^0 IP χ^2 with respect to all PVs (top left), azimuthal angle, φ (top right), transverse momentum, p_{T} (bottom left), and distance of flight (bottom right). The data are divided into 10 bins, and the value of ΔA_{CP} is measured in each bin. The last bin includes all overflow events, except in the case of φ. The horizontal red-dashed line shows the result for the combined sample. The uncertainties are statistical only. The χ^2/ndf, the corresponding p-value and the red-dashed line reported on the figures are the results of fits to the ΔA_{CP} values with a horizontal line. The central value of the fit is consistent with the baseline result. No dependencies on the variables are observed.
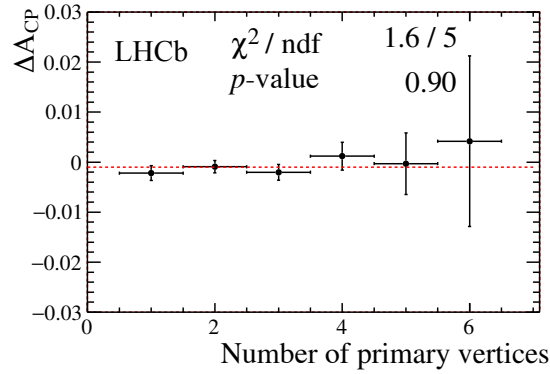
Figure 11: Dependence of ΔA_{CP} on number of reconstructed primary vertices in the event. The horizontal red-dashed line shows the result for the combined sample. The last bin includes all overflow events. The uncertainties are statistical only. The χ^2/ndf and the corresponding p-value reported on the figures are the results of a fit to the ΔA_{CP} values with a straight line. No dependence on the number of PVs is observed.
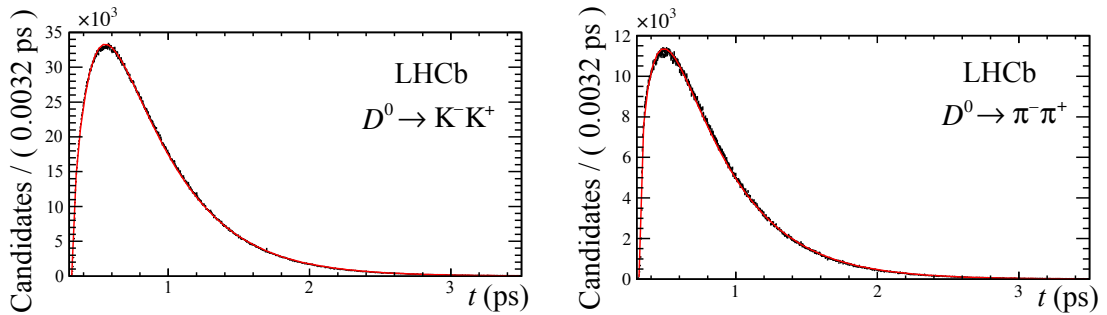

Figure 12: Decay time distribution for background-subtracted signal candidates with results from fits overlaid for (left) $D^0 \to K^- K^+$ and (right) $D^0 \to \pi^- \pi^+$ decays.